Ferromagnetism in ZnO Nanoparticles Induced by Doping of a Nonmagnetic Element: Al

ARTICLE *in* THE JOURNAL OF PHYSICAL CHEMISTRY C · JULY 2010

Impact Factor: 4.77 · DOI: 10.1021/jp103458s

Ferromagnetism in ZnO Nanoparticles Induced by Doping of a Nonmagnetic Element: Al

Daqiang Gao, Jing Zhang, Guijin Yang, Jinlin Zhang, Zhenhua Shi, Jing Qi, Zhaohui Zhang, and Desheng Xue*

Key Laboratory for Magnetism and Magnetic Materials of MOE, Lanzhou University, Lanzhou 730000, People's Republic of China

Received: April 17, 2010; Revised Manuscript Received: July 12, 2010

The room-temperature ferromagnetism of $Zn_{1-x}Al_xO$ nanoparticles synthesized by a sol−gel method is reported in this paper. X-ray diffraction and selected area electron diffraction results show that the Al atoms have successfully substituted for some of the Zn atoms in the ZnO lattice without forming other new phases. The results also show that the samples possess a typical wurtzite structure. Declaration of ferromagnetism at room temperature has been established with the observed hysteresis and the coercive field in hysteresis loops. Magnetic measurements indicate that the saturation magnetization of the samples is sensitive to the content of Al dopants and that, for $Zn_{0.97}Al_{0.03}O$, the saturation magnetization reaches the maximum of 0.012 emu/g. Combining with the results of Raman, photoluminescence, and X-ray photoelectron spectroscopies, it is suggested that the observed ferromagnetic ordering of the $Zn_{1-x}Al_xO$ nanoparticles is related to the doping-induced oxygen vacancies.

Introduction

Since the room-temperature ferromagnetism (RTFM) was observed in pure HfO_2 by Venkatesan et al.,[1] unexpected RTFM has been shown both theoretically and experimentally in a series of compounds, such as CaO,[2] CaB_6,[3] CuO,[4] and MgO.[5,6] It is suggested that magnetic properties of materials are not exclusively related to the presence of magnetic ions but can also be strongly determined by the defects, which is named as "d^0 ferromagnetism". These materials offer new approaches to designing spintronic materials that can function well above room temperature.[7] In ref 4, it is reported that the intrinsic B_6 vacancy carries the large magnetic moment of 2.4 μ_B in the CaB_6 compound. Similarly, ab initio electronic structure calculations using density functional theory indicate that the isolated Sn vacancies lead to the appearance of ferromagnetism in SnO_2.[8] Recently, it is found that carbon-doped ZnO is magnetic at room temperature via p−p interaction of C and O p orbitals.[9] More recently, Li-doped ZnO nanorods with a Curie temperature up to 554 K have been observed and investigations indicate that substitution Li atoms can induce local moments on neighboring oxygen atoms.[10] Besides, RTFM has also been reported in other nonmagnetic elements, such as Cu- and Cr-doped ZnO nanostructures.[11,12]

Al-doped ZnO is promising as a cost-effective replacement for transparent conducting oxide materials due to its excellent optical and electrical properties.[13–15] Recently, Ma et al. concluded that metallic clusters of Al might be attributed to the RTFM in the Al/ZnO film and the origin of ferromagnetism is due to the interaction of metal clusters and the ZnO matrix.[16] Chen et al. also showed that the RTFM in $(ZnO)_{1-x}/Al_x$ ($x = 0-0.5$) can be realized simply by milling a mixture of high-purity ZnO and Al fine powders for 8 h and the charge transfer between Zn and Al at the interfaces of the ball-milled nanograins may be the reason for the ferromagnetism.[17] It is known that substitution of Zn^{2+} ions by Al^{3+} ions may induce more point defects for the different ionic radii of Al^{3+} and Zn^{2+} ions.[18] If this is the case, according to the "d^0 ferromagnetism", it is expected that the RTFM can be achieved in Al-doped ZnO without Al metal clusters or the interfaces of Zn and Al. The present work reports the RTFM behavior of $Zn_{1-x}Al_xO$ nanoparticles (NPs) synthesized by the simple sol−gel method. The results indicate that ferromagnetism can be well tuned by varying the Al content. The structure and origin of the RTFM are discussed in detail.

Experimental Section

$Zn_{1-x}Al_xO$ NPs were prepared by the sol−gel method. First, 0.1 M $Zn(NO_3)_2 \cdot 6H_2O$ and yM ($y = 0$, 0.001, 0.003, and 0.005) $AlCl_3$ were dissolved in the mixed solution of ethylene glycol monomethylether ($C_3H_8O_2$) and ethylenediamine ($C_2H_8N_2$). The dissolved solution was then stirred for 4 h at 60 °C and dried to form the precursor. Finally, the precursor was annealed at 500 °C for 2 h in air and a series of the $Zn_{1-x}Al_xO$ NPs were obtained. The Al contents of $Zn_{1-x}Al_xO$ samples are nearly consistent with the starting mole percentage (0, 1, 3, and 5 atom %) used in the synthesis and were confirmed by ICP results. Parts of particles after annealing were reannealed in vacuum (10^{-3} Pa) at 500 °C for 0.5 h.

The morphologies of the NPs were characterized by a scanning electron microscope (SEM, Hitachi S-4800) and transmission electron microscope (TEM, JEM-2010). The selected area electron diffraction (SAED) and X-ray diffraction (XRD, X′ Pert PRO PHILIPS with Cu Kα radiation) were employed to study the structure of the NPs. The vibration properties were characterized by Raman scattering spectra measurements, which were performed on a Jobin-Yvon LabRam HR80 spectrometer with a 532 nm line of a Torus 50 mW diode-pumped solid-state laser under backscattering geometry. X-ray photoelectron spectroscopy (XPS, VG ESCALAB 210) was utilized to determine the bonding characteristics and the composition of the particles. The composition was also confirmed by an inductively coupled plasma atomic emission spectrometer (ICP, ER/S). Microphotoluminescence (PL) mea-

* To whom correspondence should be addressed. E-mail: xueds@lzu.edu.cn.

10.1021/jp103458s
Published on Web 07/26/2010

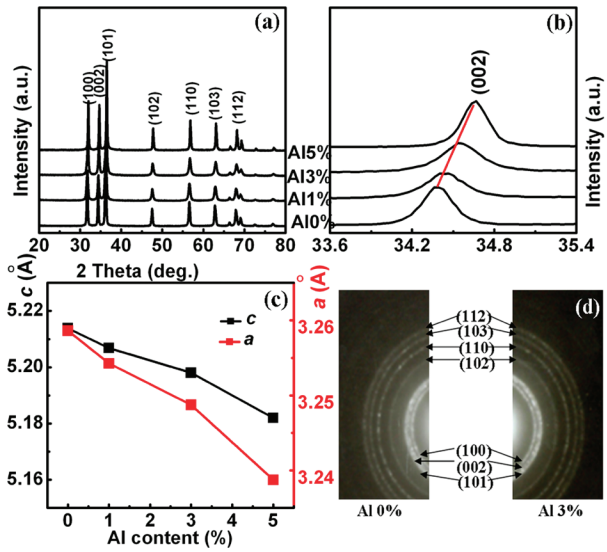

Figure 1. (a) XRD patterns of $Zn_{1-x}Al_xO$ NPs. (b) XRD patterns of $Zn_{1-x}Al_xO$ NPs in detail. (c) The variation of *c* dependence on the Al content in ZnO NPs. (d) The SAED of ZnO and $Zn_{0.97}Al_{0.03}O$ NPs.

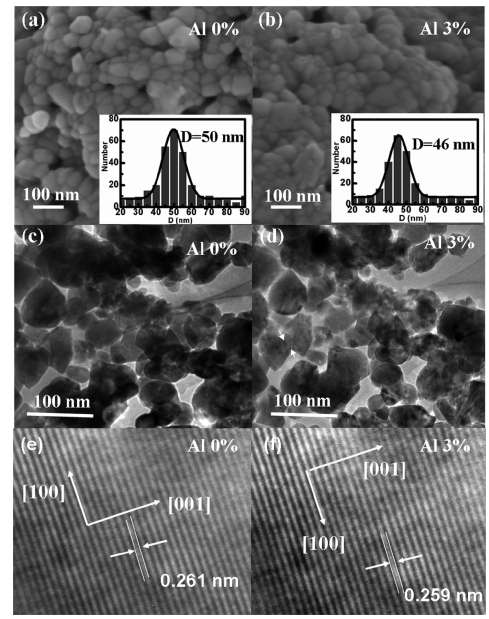

Figure 2. SEM images of (a) ZnO and (b) $Zn_{0.97}Al_{0.03}O$, TEM images of (c) ZnO and (d) $Zn_{0.97}Al_{0.03}O$, and HRTEM images of (e) ZnO and (f) $Zn_{0.97}Al_{0.03}O$ NPs. The insets in (a) and (b) are the size distribution plots of the ZnO and $Zn_{0.97}Al_{0.03}O$ NPs.

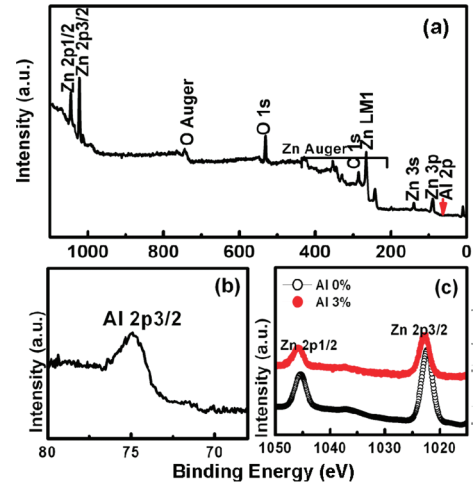

Figure 3. (a) XPS survey spectrum and high-resolution scans of (b) Al 2p of $Zn_{0.97}Al_{0.03}O$ NPs and (c) Zn 2p of ZnO and $Zn_{0.97}Al_{0.03}O$ NPs.

surements were carried out at room temperature using a He−Cd laser with a wavelength of 325 nm and output power of 15 W as the excitation source. The measurements of magnetic properties were made using the vibrating sample magnetometer (VSM, Lakeshore 7304) and the Quantum Design MPMS magnetometer based on a superconducting quantum interference device (SQUID).

Results and Discussion

The representative XRD patterns of $Zn_{1-x}Al_xO$ NPs with $x = 0$, 0.01, 0.03, and 0.05 are shown in Figure 1a. The results indicate that all of the samples have the hexagonal wurtzite structure (JCPDS card no. 36-1451). Additional reflections are not observed even for the particles containing the largest amount of Al, indicating that there is no additional phase presenting in the samples. A detectable slight shift toward the larger angle occurs with increasing the Al doping content, as shown in Figure 1b. The lattice parameters *c* and *a* decrease monotonously with increasing the Al content (shown in Figure 1c). Considering the difference of the ionic radii in Al^{3+} and Zn^{2+} ions (Zn^{2+} ∼ 0.74 Å, Al^{3+}∼ 0.54 Å),[19] these results suggest a homogeneous doping of Al atoms that substitute for Zn ions. Simultaneously, as can be seen from Figure 1d, SAED patterns of both ZnO and $Zn_{0.97}Al_{0.03}O$ NPs show that there is no Al or oxide cluster formation in $Zn_{0.97}Al_{0.03}O$ NPs. Hence, we can conclude that there is no other impurity phase in the Al-doped ZnO NPs and Al ions are doped into the ZnO lattice by substituting for Zn ions

Figure 2a,b shows the SEM images of ZnO and $Zn_{0.97}Al_{0.03}O$ NPs. It is clearly seen that all of the NPs are accumulated together. The size distribution plots for the two samples are shown in the insets of the corresponding images, which reveal that the average particle sizes are 50 and 46 nm for ZnO and $Zn_{0.97}Al_{0.03}O$ NPs, respectively. Figure 2c,d shows the TEM images of ZnO and $Zn_{0.97}Al_{0.03}O$ NPs. The average sizes of these particles correspond to the results of SEM. The high-resolution transmission electron microscopy (HRTEM) images of ZnO and $Zn_{0.97}Al_{0.03}O$ NPs are shown in Figure 2e,f, respectively. The distance between adjacent lattice fringes of (002) planes from the HRTEM image for $Zn_{0.97}Al_{0.03}O$ NPs is about 0.259 nm, which is smaller than that of ZnO (about 0.261 nm, as shown in Figure 2e). Meanwhile, the difference between the adjacent lattice fringe distance of $Zn_{0.97}Al_{0.03}O$ and ZnO is considered to be caused by the substituting for Zn ions by Al, which corresponds to the results of XRD.

The chemical states of the compositional elements in $Zn_{1-x}Al_xO$ NPs were revealed by XPS, and a representative spectrum of $Zn_{0.97}Al_{0.03}O$ NPs is shown in Figure 3. Panels a−c in Figure 3 are the survey spectrum and Al 2p and Zn 2p core-level spectra, respectively. As shown in Figure 3a, the indexed peaks only correspond to elements Zn, O, Al, and C. The peak located at 74.3 eV is identified with the binding energies of Al^{3+} shown in Figure 3b.[20] The result of the Zn 2p core-level XPS spectrum for ZnO (Figure 3c) shows that the doublet spectral lines of Zn 2p are observed at the binding energies of 1022 eV (Zn $2p_{3/2}$) and 1045 eV (Zn $2p_{1/2}$) with a spin−orbit splitting of 23 eV, which coincides with the results for Zn^{2+} in ZnO.[21] A slightly detectable shift toward the larger binding energy of about 0.9 eV than that of pure ZnO is observed for

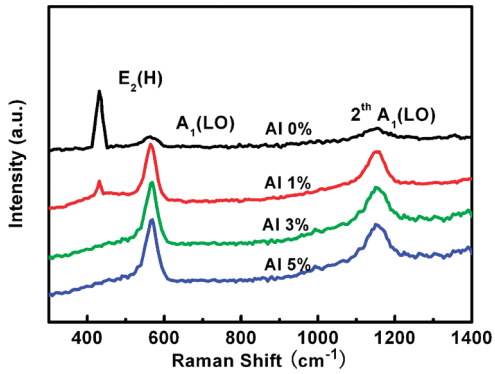

Figure 4. Raman spectra of $Zn_{1-x}Al_xO$ NPs.

$Zn_{0.97}Al_{0.03}O$ NPs, which may be caused by the substituting of Al ions for Zn ions.

The additional information on the structure of $Zn_{1-x}Al_xO$ NPs was obtained by Raman spectroscopy. Figure 4 shows the room-temperature Raman spectra of the $Zn_{1-x}Al_xO$ samples at the range of 200−1400 cm^{-1}. The sharpest and strongest peak around 437 cm^{-1} can be assigned to the nonpolar optical phonon E_2 (high) mode of ZnO, which is a typical Raman active branch of wurtzite ZnO.[22] The presence of the E_2 (high) mode in all samples indicates the hexagonal wurtzite structure of $Zn_{1-x}Al_xO$, which is in good agreement with the HRTEM and XRD observations. Besides, an additional mode located at 574 cm^{-1} and identified as the A_1 (LO) phonon mode also can be observed, which is associated with the defects of O vacancies, Zn interstitials, or their complexes.[23] The peak at 1164 cm^{-1} was just a second-order peak of the LO phonon. It can be seen that, as the Al content increases, the intensity of the A_1 (LO) peak increases while the E_2 (high) one decreases gradually, which reveals that more defects are introduced in these samples by the doping of Al. Meanwhile, the contrasts in defect contents in samples of $Zn_{1-x}Al_xO$ motivated us to carry out a comparative study on their magnetic properties according to the "d^0 ferromagnetism".[1−12]

Magnetization curves as a function of applied magnetic field ($M-H$) at 300 K for $Zn_{1-x}Al_xO$ samples are shown in Figure 5a, where the contributions of the paramagnetism (PM) signal of the samples were deducted. The magnification of the central part for the $M-H$ curves is shown in the inset of Figure 5a. It can be seen that all of the samples with $x = 0-0.05$ exhibit a hysteresis curve with different coercivities and saturation magnetization (M_s), which indicates that all of the samples have the RTFM. The M_s for the pure ZnO NPs is about 0.0015 emu/g, which may be caused by the unpaired electron spins on the surface of the particles or the defect of surface. Apparently, the magnetism of the samples strongly depends on the doping content for Al-doped ZnO NPs. It can be seen that M_s increases with x increasing before reaching 0.03 but decreases abruptly after reaching 0.03. This kind of variation trend in M_s as a function of nonmagnetic ion concentration is similar to what has been previously reported in Cu-doped SnO_2.[24] The consistent drop in M_s at higher Al contents could be due to the increasing occurrence of antiferromagnetic coupling between Al pairs occurring at shorter separated distances, which was similar to the system of Cr- and Er-doped ZnO.[25,26] We also performed the magnetic property measurement of $Zn_{0.97}Al_{0.03}O$ NPs at low temperatures. The $M-H$ curves (half of the curve) of $Zn_{0.97}Al_{0.03}O$ NPs at 10−250 K are shown in Figure 5b, where the PM signal contribution due to the holder has also been subtracted. The $M-H$ curves show that there is considerable

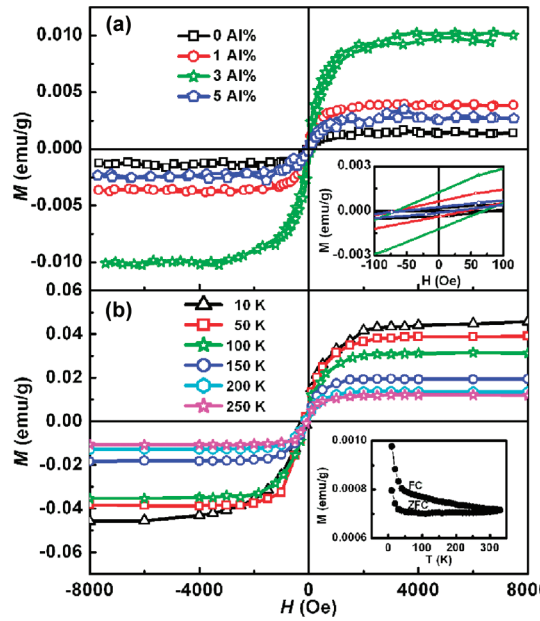

Figure 5. (a) $M-H$ curves of $Zn_{1-x}Al_xO$ NPs at room temperature and (b) $M-H$ curves of $Zn_{0.97}Al_{0.03}O$ NPs at the low temperatures of 10−250 K. The insets in (a) and (b) are the magnification of the central part of the $M-H$ curves and the FC-ZFC curve of $Zn_{0.97}Al_{0.03}O$ NPs, respectively.

hysteresis and the coercive field decreases monotonically with temperature, which is a typical behavior of ferromagnetic materials.

If there is any contamination of the ferromagnetic cluster formation in $Zn_{1-x}Al_xO$ NPs, it is expected that the $Zn_{0.97}Al_{0.03}O$ nanaparticle has the most because of its highest M_s. However, the zero-field-cooled (ZFC) and field-cooled (FC) magnetization curves at the dc field of 100 Oe on this sample show that there is no blocking temperature in the temperature range of 2−330 K (shown in the inset of Figure 5b). At the same time, there are no other elements (such as Fe, Co) that exist in the test precision of both XPS and ICP, so the ferromagnetic contamination can be ruled out. It can also be concluded that the Curie temperature of this sample is above 330 K. Therefore, the observed ferromagnetism of the $Zn_{1-x}Al_xO$ NPs should be the intrinsic nature of the material and the ferromagnetic ordering in Al-doped ZnO NPs may be explained by the defect-induced "d^0 ferromagnetism".

To explore the kind of defect, PL measurements were preformed for $Zn_{1-x}Al_xO$ NPs, and the results are shown in Figure 6a. It can be seen that all of the samples exhibit a strong and broad deep level emission (DLE) peak in the visible region, where it is ascribed to the transitions of the excited optical centers from the deep levels to the valence band, and these deep levels are associated with the intrinsic oxygen vacancies.[27] Coupled with the decreasing of the intensity of the near-band-edge (NBE) UV peak, the intensity of the DLE peak increases gradually with the increase of Al content in ZnO NPs, so it can be concluded that the oxygen vacancies are dominant in our samples and more oxygen vacancies are produced by the introduction of Al. In addition, the typical O 1s spectra corresponding to samples of ZnO and $Zn_{0.97}Al_{0.03}O$ are shown in Figure 6b and are fitted with three Gaussian peaks marked as Oa, Ob, and Oc, as reported in the literature.[28,29] Generally, the peak marked as Oc is attributed to the O^{2-} ions in the wurtzite structure of ZnO. The higher binding energy component Oa is usually attributed to the loosely bound oxygen species

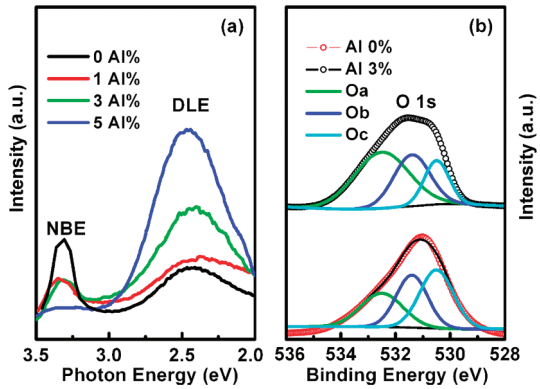

Figure 6. (a) PL spectra of the $Zn_{1-x}Al_xO$ NPs measured at room temperature. (b) XPS spectra of O 1s corresponding to ZnO and $Zn_{0.97}Al_{0.03}O$ NPs. The peak indicated as Ob corresponds to the O vacancy.

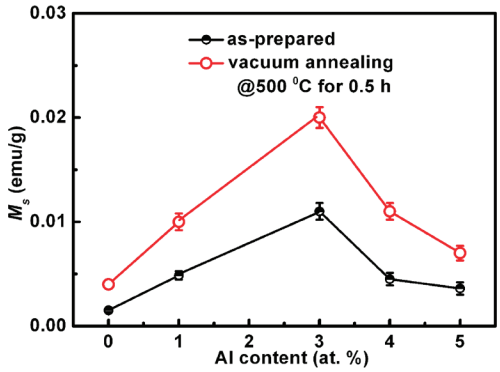

Figure 7. Variation of M_s for $Zn_{1-x}Al_xO$ NPs before and after reannealing in vacuum (10^{-3} Pa).

on the surface of the particles belonging to adsorbed $-CO_3$, H_2O, or O_2. Meanwhile, it has been previously reported that the peak marked as Ob for a binding energy of 531.2 eV is associated with the loss of oxygen (O vacancies) within the ZnO matrix,[28,29] where the variation in relative area under this peak indicates the variation of O vacancies in the samples. Here, the relative areas of Ob for ZnO and $Zn_{0.97}Al_{0.03}O$ are about 22% and 31%, respectively, implying that the doping of Al can introduce more oxygen vacancies in our case, which corresponds to the result of PL. At the same time, these results alert us that the oxygen vacancies may play an important role in introducing RTFM in $Zn_{1-x}Al_xO$ NPs.

To confirm this further, the effect of isochronal annealing under a reduced pressure (10^{-3} Pa) on the magnetic properties was investigated, and the results are shown in Figure 7. It can be seen that the M_s increased for all $Zn_{1-x}Al_xO$ NPs after vacuum annealing at 500 °C for 0.5 h. It is well known that vacuum annealing results in the higher population density of oxygen vacancies in oxides due to the deficiency of oxygen. Therefore, the enhancement of M_s for $Zn_{1-x}Al_xO$ NPs upon vacuum annealing could be attributed to a higher density of oxygen vacancies, which is most likely at the surface/or interface of the nanostructured ZnO grains. In Figure 7, the high value of M_s for sample $Zn_{0.97}Al_{0.03}O$ remains after vacuum annealing, which suggests that both the content of Al in ZnO and oxygen vacancies of the samples are related to the observed ferromagnetism.

Recently, RTFM was observed in semiconductors or oxides doped with nonmagnetic elements[30] as well as undoped oxides, such as ZnO, In_2O_3, and HfO_2,[31,32] and the ferromagnetic properties of these materials are strongly dependent on sample preparation. The correlation between ferromagnetism and sample preparation conditions suggests that defects may play an important role in the observed magnetic behaviors of these materials. Therefore, how to control defects is a very interesting and challenging issue. It is suggested that cation vacancies often have a higher formation energy than oxygen vacancies and can form only in oxygen-rich environments.[33] A high content of oxygen vacancies could also promote the probable formation of anionic vacancy clusters, which can induce sizable magnetic moments.[34] Here, our experiments were carried out in oxygen-poor conditions where the oxygen deficiency always contributes to the nonstoichiometry.[35] PL and O 1s fitting results indicate that oxygen vacancies are dominant in our samples and more oxygen vacancies are produced by the introduction of Al. Besides, vacuum annealing can enhance the ferromagnetism of the samples, so the tunable RTFM in Al-doped ZnO NPs confirms that oxygen vacancies play a critical role to ferromagnetism. NPs have a large surface-to-volume ratio. Consequently, a large number of surface defects are generated, and the RTFM was introduced even in pure oxide.[36,37] Owing to having different ionic radii and valence states, Al ions doped into the ZnO lattice by substituting for Zn ions may lead to more oxygen vacancies in samples. The donor impurity band exchange model explained[38] that point defects, such as oxygen vacancies, are responsible for formation of bound magnetic polarons (BMPs). Defect-induced shallow levels hybridize with the d level of transition-metal ions and subsequently stabilize the ferromagnetic ordering in diluted magnetic oxides. More study is needed to confirm our opinion.

Conclusions

Intrinsic RTFM is initially reported in nonmagnetic ion Al-doped ZnO NPs synthesized by the sol−gel method. It is found that the M_s of the $Zn_{1-x}Al_xO$ NPs is sensitive to the Al doping content and the highest M_s appears in the NPs with a moderate Al content of 3 atom %. Raman, photoluminescence, and O 1s fitting results suggested that the observed ferromagnetism in the $Zn_{1-x}Al_xO$ NPs is related to the doping-induced oxygen vacancies. The present study not only demonstrates that Al-doped ZnO NPs show RTFM but also suggests that introducing oxygen vacancies is the effective way to boost the d^0 ferromagnetism.

Acknowledgment. This work is supported by the National Science Fund for Distinguished Young Scholars (Grant No. 50925103), The Key Grant Project of the Chinese Ministry of Education (Grant No. 309027), the NSFC (Grant No. 50902065), and the Fundamental Research Funds for the Central Universities (Grant No. Lzujbky-2009-162).

References and Notes

(1) Venkatesan, M.; Fitzgerald, C. B.; Coey, J. M. D. *Nature* **2004**, *430*, 630.
(2) Elfimov, I. S.; Yunoki, S.; Sawatzky, G. A. *Phys. Rev. Lett.* **2002**, *89*, 216403.
(3) Das Pemmaraju, C.; Sanvito, S. *Phys. Rev. Lett.* **2005**, *94*, 217205.
(4) Shang, D. J.; Yu, K.; Zhang, Y. S.; Xu, J. W.; Wu, J.; Xu, Y.; Li, L. J.; Zhu, Z. Q. *Appl. Surf. Sci.* **2009**, *255*, 4093.
(5) Gallego, S.; Beltrán, J. I.; Cerdá, J.; Muñoz, M. C. *J. Phys: Condens. Matter* **2005**, *17*, L451.
(6) Hu, J. F.; Zhang, Z. L.; Zhao, M.; Qin, H. W.; Jiang, M. H. *Appl. Phys. Lett.* **2008**, *93*, 192503.
(7) Peng, H. W.; Xiang, H. J.; Wei, S. H.; Li, S. S.; Xia, J. B.; Li, J. B. *Phys. Rev. Lett.* **2009**, *102*, 017201.
(8) Gul, R.; Víctor, M.; García, S.; Hong, S. C. *Phys. Rev. B* **2008**, *78*, 184404.
(9) Pan, H.; Yi, J. B.; Shen, L.; Wu, R. Q.; Yang, J. H.; Lin, J. Y.; Feng, Y. P.; Ding, J.; Van, L. H.; Yin, J. H. *Phys. Rev. Lett.* **2007**, *99*, 127201.

(10) Chawla, S.; Jayanthi, K.; Kotnala, R. K. *Phys. Rev. B* **2009**, *79*, 125204.

(11) Gao, D. Q.; Xu, Y.; Zhang, Z. H.; Gao, H.; Xue, D. S. *J. Appl. Phys.* **2009**, *105*, 063903.

(12) Xu, C. K.; Yang, K. K.; Liu, Y. Y.; Huang, L. W.; Lee, H.; Cho, J. H.; Wang, H. *J. Phys. Chem. C* **2008**, *112*, 19236.

(13) Jin, Z. C.; Hamberg, I.; Granqvist, C. G. *J. Appl. Phys.* **1988**, *64*, 5117.

(14) Yoo, J. B.; Fahrenbruch, A. L.; Bube, R. H. *J. Appl. Phys.* **1990**, *68*, 4694.

(15) Major, S.; Kumar, S.; Bhatnagar, M.; Chopra, K. L. *Appl. Phys. Lett.* **1986**, *49*, 394.

(16) Ma, Y. W.; Ding, J.; Qi, D. C.; Yi, J. B.; Fan, H. M.; Gong, H.; Wee, A. T. S.; Rusydi, A. *Appl. Phys. Lett.* **2009**, *95*, 072501.

(17) Chen, S. J.; Suzuki, K.; Garitaonandia, J. S. *Appl. Phys. Lett.* **2009**, *95*, 172507.

(18) Klingshirn, C. *Phys. Status Solidi B* **2007**, *244*, 3027.

(19) Zhou, B.; Wu, Y. S.; Wu, L. L.; Zou, K.; Gai, H. D. *Physica E* **2009**, *41*, 705.

(20) Chen, M.; Wang, X.; Yu, Y. H.; Pei, Z. L.; Bai, X. D.; Sun, C.; Huang, R. F.; Wen, L. S. *Appl. Surf. Sci.* **2000**, *158*, 134.

(21) Moulder, J. F.; Stickle, W. F.; Sobol, P. E.; Bomben, K. D. In *Handbook of X-ray Photoelectron Spectroscopy*; Chastain, J., Kings, R. C., Jr., Eds.; Physical Electronics Inc.: Eden Prarie, MN, 1995.

(22) Jeong, S. H.; Kim, J. K.; Lee, B. T. *J. Phys. D: Appl. Phys.* **2003**, *36*, 2017.

(23) Pradhan, A. K.; Zhang, K.; Loutts, G. B.; Roy, U. N.; Cui, Y.; Burger, A. *J. Phys.: Condens. Matter* **2004**, *16*, 7123.

(24) Li, L. J.; Yu, K.; Tang, Z.; Zhu, Z. Q.; Wan, Q. *J. Appl. Phys.* **2010**, *101*, 014303.

(25) Zhuge, L. J.; Wu, X. M.; Wu, Z. F.; Chen, X. M.; Meng, Y. D. *Scr. Mater.* **2009**, *60*, 214.

(26) Qi, J.; Yang, Y. H.; Zhang, L.; Chi, J. H.; Gao, D. Q.; Xue, D. S. *Scr. Mater.* **2009**, *60*, 289.

(27) Xing, G. Z.; Wang, D. D.; Yi, J. B.; Yang, L. L.; Gao, M.; He, M.; Yang, J. H.; Zhao, Q. X.; Ding, J.; Sum, T. C.; Wu, T. *Appl. Phys. Lett.* **2010**, *96*, 112511.

(28) Zhang, L.; Ge, S. H.; Zuo, Y. L.; Zhang, B. M.; Xi, L. *J. Phys. Chem. C* **2010**, *114*, 7541.

(29) Pandey, B.; Ghosh, S.; Srivastava, P.; Kumar, P.; Kanjilal, D.; Zhou, S.; Schmidt, H. *J. Appl. Phys.* **2010**, *107*, 023901.

(30) Pan, H.; Yi, J. B.; Shen, L.; Wu, R. Q.; Yang, J. H.; Lin, J. Y.; Feng, Y. P.; Ding, J.; Van, L. H.; Yin, J. H. *Phys. Rev. Lett.* **2007**, *99*, 127201.

(31) Hong, N. H.; Sakai, J.; Poirot, N.; Brize, V. *Phys. Rev. B* **2006**, *73*, 132404.

(32) Sundaresan, A.; Bhargavi, R.; Rangarajan, N.; Siddesh, U.; Rao, C. N. R. *Phys. Rev. B* **2006**, *74*, 161306.

(33) Oba, F.; Nishitani, S. R.; Isotani, S.; Adachi, H.; Tanaka, I. *J. Appl. Phys.* **2001**, *90*, 824.

(34) Banerjee, S.; Mandal, M.; Gayathri, N.; Sardar, M. *Appl. Phys. Lett.* **2007**, *91*, 182501.

(35) Oba, F.; Togo, A.; Tanaka, I.; Paier, J.; Kresse, G. *Phys. Rev. B* **2008**, *77*, 245202.

(36) Darshana, Y. I.; Amit, D. L.; Arjun, K. P.; Igor, D.; Naushad, A.; Shailaja, M. *J. Phys. Chem. C* **2010**, *114*, 1451.

(37) Gao, D. Q.; Zhang, Z. H.; Fu, J. L.; Xu, Y.; Qi, J.; Xue, D. S. *J. Appl. Phys.* **2009**, *105*, 113928.

(38) Mukadam, M. D.; Yusuf, S. M.; Sasikala, R.; Kulshreshtha, S. K. *J. Appl. Phys.* **2006**, *99*, 034310.

JP103458S